Fast operating moving coil actuator for a vacuum interrupter

X. Pei, A. C. Smith, *Senior Member, IEEE,* R. Shuttleworth, *Member, IEEE,* D. S. Vilchis-Rodriguez, and M. Barnes, *Senior Member, IEEE*

***Abstract*--Vacuum circuit breakers are the dominant technology in medium voltage distribution networks since they are environmentally friendly and maintenance free. It is a challenge to design an actuator for a vacuum circuit breaker, which achieves a high operating speed whilst maintaining high efficiency. A fast operating moving coil actuator for a vacuum interrupter (VI) has been developed. An analytical model of the actuator was initially developed and then simulated using a three-dimensional finite element (FE) model. The model showed that the opening force was higher than the closing force due to asymmetry in the structure of the actuator, which resulted in a reluctance force component. The complete operating actuator prototype was built to avoid known problems such as contact popping, bounce, rebound and welding.**

The magnetic field distribution and the static electromagnetic force on the moving coil were measured and provided a good correlation with the FE model simulation predications. The opening operation of the actuator prototype was compared for different capacitor supply voltages. A maximum velocity of 2.3 m/s was achieved when the capacitor was charged to 150 V. The actuator demonstrated successful operation at atmospheric pressure and also in a vacuum chamber. The opening time of the actuator in the vacuum was approximately 5 ms, compared to 5.5 ms at atmospheric pressure. We designed and built this actuator to illustrate that the moving coil actuator is capable to operate the vacuum circuit breaker quickly with high efficiency. Tests showed that further design optimizations for improving the operating speed and efficiency of the moving coil actuator are essential and the options have also been suggested.

***Index Terms*--Finite element, Moving coil actuator, Nd-Fe-B permanent magnet, Vacuum interrupter.**

I. Introduction

SULFUR hexafluoride (SF_6) and vacuum circuit breakers have already replaced the previous air and oil solutions and have become the most widely used options. Vacuum circuit breakers are being increasingly used in medium voltage distribution networks since their commercialization in the 1970's. Vacuum interrupters offer advantages of being environmentally friendly, reduced maintenance, compactness, rapid dielectric recovery of the vacuum and less operating energy than SF_6 circuit breakers [1]. The design and build of a fast-acting actuator for a vacuum interrupter (VI) is important for many applications in medium voltage distribution networks such as power system protection and superconducting fault current limiters (SFCL) incorporating a VI [2-4].

A VI needs a comparatively short contact stroke. The actuator is required to compress the contacts together with a considerable force to prevent the contacts from separating during normal operation [5]. There are three main types of VI actuator available: spring actuator [6, 7], solenoid actuator [8-11] and permanent magnetic actuator [12-14]. The structure of the spring actuator is complex and they have a large number of components which causes problems in terms of reliability and maintenance [12]. The solenoid actuator is simple and has a robust structure. The solenoid coil however needs to be energized continuously to hold the movable contact in the open or closed positions; otherwise a latch mechanism is required [11]. Permanent magnetic actuators provide reliable operation with a compact structure. The operating speed however is limited by the heavy armature and induced eddy currents. Alternatively, the Thomson coil actuator using an electromagnetic repulsion mechanism also has been investigated over the past decade [15-19]. The operating velocity of the Thomson coil actuator can be as high as 8 m/s but the energy conversion efficiency is limited in the 5-14% range [17]. The energy conversion efficiency of the magnetic actuator is defined as the output mechanical energy divided by the input electrical energy. Finite element analysis has been conducted to improve the efficiency of the Thomson coil actuator [19].

A moving coil actuator composed of a lightweight moving coil, permanent magnets and mild steel blocks is proposed and investigated in this paper. This type of actuator has been widely used in loudspeakers and disk drive read heads for several decades [20, 21]. The moving coil actuator has the advantages of quick response time and low moving mass, which are beneficial attributes for a VI actuator. Furthermore, the efficiency of the moving coil actuator is generally higher than that of the Thomson coil actuator for a similar stroke length [22].

This paper presents the work conducted on the design, build and test of the moving coil actuator. The structure of this paper is as follows. Section II introduces the VI specification and requirements for the fast operation of the VI actuator. Section III presents the analytical and finite element (FE) modeling of the moving coil actuator. The design of the magnetic latches and final operational actuator are also included. Section IV

This work was funded as part of the UK EPSRC, FCL/CB: An Integrated VSC-HVDC Fault Current Limiter/Breaker project, EP/L021552/1.

X. Pei is with the Department of Electronic and Electrical Engineering, The University of Bath, Bath, BA2 7AY, U.K. (e-mail: x.pei@bath.ac.uk).

A. C. Smith, R. Shuttleworth, D. S. Vilchis-Rodriguez and M. Barnes are with the Power and Energy Division, School of Electrical and Electronic Engineering, The University of Manchester, Manchester, M13 9PL, U. K.

describes the experimental setup and validation compared with the modeling. The opening operation of the moving coil actuator was tested and compared at atmospheric pressure and in a vacuum chamber. This main objective of this paper is to give an overview of the moving coil actuator design and identify the potential improvements for medium voltage distribution network applications.

II. Vacuum Interrupter and Actuator Requirements

A commercial DVS10CB VI was investigated as an example in this paper. The specification of the investigated VI is outlined in Table I. The rated current of the DVS10CB VI is 320 A. The separation distance between contacts is 2 mm and the maximum operating voltage is 1.5 kV. This VI is used for a vacuum circuit breaker; the actuator therefore has to provide a latching function in the open and closed positions. In the closed position, a minimum holding force of 2 kgf is required to reduce the contact resistance at the maximum interrupting current of 3.2 kA. The total movement of the actuator was designed to be 5 mm: 3 mm further than the stroke of the vacuum circuit breaker to compensate for contact wear.

The overall design requirements of the vacuum circuit breaker actuator are listed as follows:

- Linear displacement of 5 mm;
- Provide fast operation (less than 5 ms);
- Light moving mass;
- Latch function in the open and closed positions with adequate holding force; and
- Reasonable size, weight and efficiency.

TABLE I: DVS10CB vacuum circuit breaker specification

Parameter	Rated value
Maximum operating voltage	1.5 kV
Stroke	2 mm
Rated AC current	320 A
Maximum interrupting current	3.2 kA
Contact holding force for 3.2 kA	2 kgf

III. Modeling and Design

The moving coil actuator has a similar operating principle to a loudspeaker coil: a light, hollow coil is suspended in a strong radial magnetic field to allow free movement along the axial direction. Circumferential current flow in the coil then produces an axial force on the coil, which drives the coil along the axial direction [20, 21].

The moving coil actuator is composed of a set of steel blocks, permanent magnets and a copper-wound coil. It was difficult to obtain annular permanent magnets of suitable size with a radial magnetized field. Therefore, four rectangular blocks of permanent magnets with an internal arc surface facing the airgap were used to keep the radial length of the airgap small. Four steel walls, a bottom steel block and a steel cylinder inside the actuator coil provided the low reluctance path for the magnetic flux produced by the magnets. The four magnets were attached to the outer steel walls and the actuator coil placed in the airgap between the magnets and the steel cylinder. The cutaway geometry of the actuator is shown in Fig. 1. The two steel walls at the front of Fig. 1 are hidden to show the detail in the middle of the actuator. The blocks in grey and black represent the steel and permanent magnets, respectively, whilst the ring in pink represents the actuator coil.

A. Analytical model

A preliminary analytical model was initially built to determine the baseline parameters of the actuator using a classical magnetic circuit model. Fig. 2 shows a simplified actuator model in the cross section through the center of one of the magnets. The approximate magnetic flux density in the airgap could be calculated using Ampere's Law along the red line, which denotes the mean flux path of the magnetic circuit.

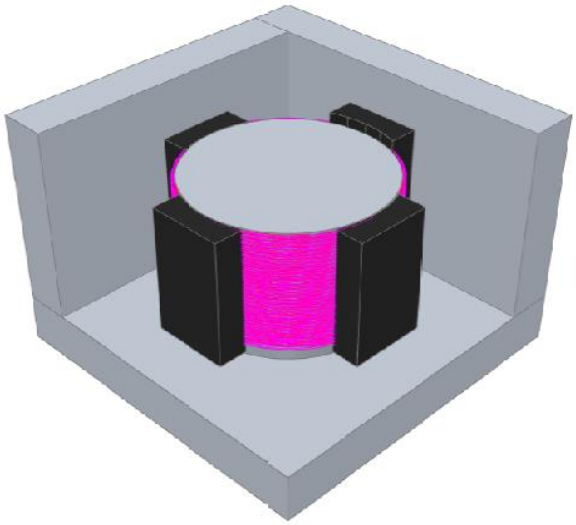

Fig. 1. Cutaway geometry of the actuator (grey: mild steel; black: magnets; pink: coil).

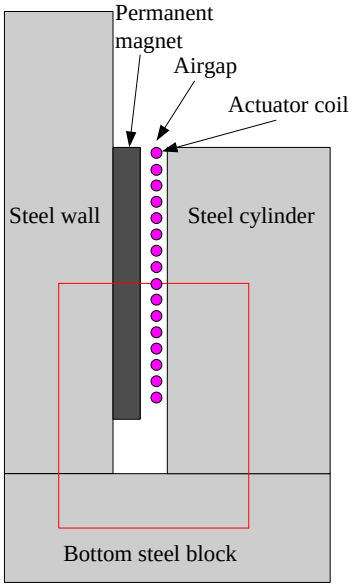

Fig. 2. Simplified model of the magnetic circuit

The operating point of the magnet in the model shown in Fig. 2 can be further simplified using the following assumptions: the permeability of steel is assumed to be infinite and hence the reluctance of the steel can be neglected; and

there are no flux leakage and fringing effects in the magnetic circuit. The magnetic flux density of the magnet at the operating point can be expressed as:

$$B_m = \frac{B_r}{1+\mu_m\left(\frac{l_g}{l_m}\right)} \quad (1)$$

where B_r is the remanence in the permanent magnet, μ_m is the relative permeability of the magnet, l_g and l_m is the thickness of the airgap and the magnet, respectively.

The actuator coil is situated in a radial magnetic field produced by the magnets. An electromagnetic force is generated on the coil when an electrical current flows through the coil. This electromagnetic force is also called Lorentz force F:

$$\mathrm{F} = I\int dl \times B \quad (2)$$

where I is the current in the coil and B is the magnetic field density produced by the magnets passing through the coil.

When the coil is moved by the Lorentz force along the axial direction, an electromotive force (emf) is produced on the moving coil and is expressed as:

$$\varepsilon = \oint_C (v\times B)\cdot dl \quad (3)$$

where ε is the electromotive force and v is the velocity of the moving coil.

It is assumed that the actuator coil is supplied by a pre-charged capacitor. The current through the coil can be calculated as:

$$L\frac{di}{dt} + Ri = U - \varepsilon \quad (4)$$

where L is the inductance of the coil, R is the resistance of the coil, i is the current flow through the coil, and U is the capacitor voltage.

The efficiency of the moving coil actuator (η) can be estimated by:

$$\eta = \frac{mv_1^2}{C(U_{co}^2 - U_{c1}^2)} \quad (5)$$

where m is the mass of the actuator moving part, v_1 is the maximum velocity of the actuator, C is the capacitance, U_{co} is the initial voltage across the capacitor, and U_{c1} is the voltage across the capacitor when the moving coil is at the maximum velocity.

The above equations were used to define the baseline of the moving coil actuator geometry to be used in the FE model. The size of the key components for the prototype actuator is listed in Table II. N48 neodymium-iron-boron (Nd-Fe-B) rare-earth permanent magnet has a remanence of 1.4 T and the magnetic flux density of the magnet at the operating point is designed to be 1 T using equation (1). If it is assumed that the maximum actuator current is 50 A, the total force on the actuator coil would theoretically be 790 N.

TABLE II: Parameters of the key components for the actuator

Item	Material	Size (mm)	
Permanent magnet	N48 Nd-Fe-B magnet	80×50×15.3	
Steel wall	EN1A steel	198×120×30	
Bottom steel block	EN1A steel	228×228×30	
Steel cylinder	EN1A steel	Radius	63
		Height	88
Actuator coil	AWG 19 copper wire	Radius	66
		Height	75

B. Finite element model

A 3-D FE model of the moving coil actuator was developed based on the parameter listed in Table II using the Vector Fields Opera software. The symmetrical structure of the moving coil actuator with respect to the YZ and ZX planes allowed the 3-D FE model to be reduced to one quarter segment significantly reducing the computational solution time. The magnetic field produced by the magnets was simulated by setting the current density in the actuator coil to zero.

Fig. 3 shows a 3-D plot of the flux density distribution produced by the permanent magnets. The magnetic flux is unevenly distributed in the steel walls and cylinder along the Z-axis due to the non-symmetrical structure. It is clear from Fig. 3 that the flux density in the steel blocks close to the bottom edge of the magnets is close to the saturation point of the magnetic steel. However, the magnetic flux levels at the top section of the steel walls are low and therefore could be removed to reduce the overall weight.

Fig. 4 shows the flux density at the midway point of the airgap and the four magnet poles are clearly evident. The maximum flux density in the airgap was found to be 0.965 T, which confirms that the maximum flux density calculated from the analytical model of 1 T is reasonable. The magnetic flux density in the airgap reduces rapidly from the edge of the magnets. It should be pointed out that only the coil section within the magnetic field develops the electromagnetic force when a current is applied. The average flux density across the whole airgap surface is 0.45 T.

Fig. 5 shows the magnitude of the flux density in the airgap along the vertical path marked on Fig. 3. The path is located at the center of one of the magnet arcs and the midway point in the airgap between the magnet and the steel cylinder. The flux density, as expected, is relatively constant at the center of the magnet but reduces slightly at both ends due to flux leakage and fringing effects. The average flux density along the path is approximately 0.9 T.

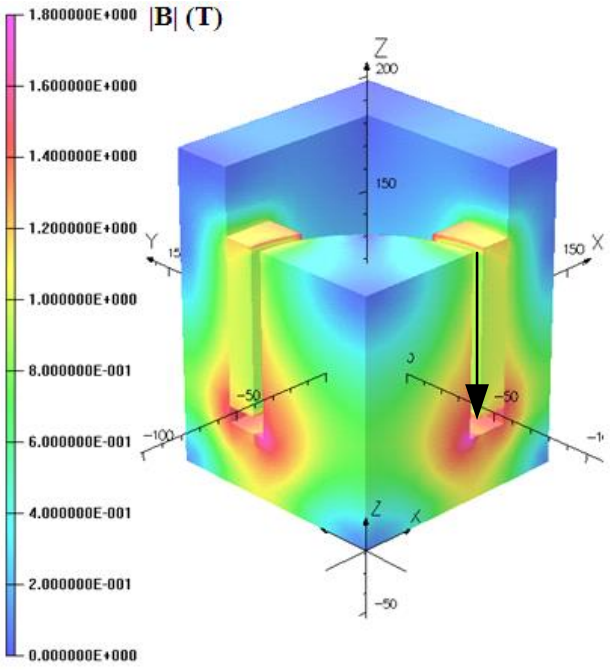

Fig. 3. 3-D plot of the flux density distribution produced by the magnets.

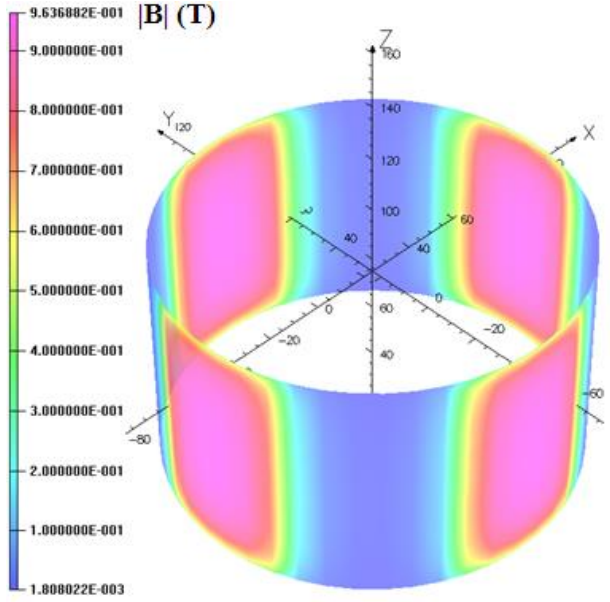

Fig. 4. Flux density distribution in the airgap produced by the magnets.

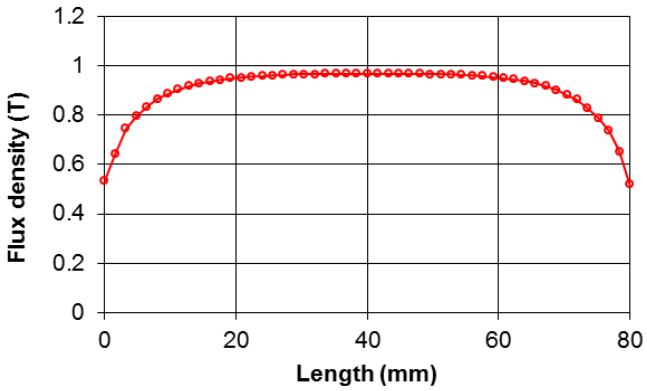

Fig. 5. Flux density distribution in the airgap produced by the magnets (along the vertical path shown in Fig. 3).

The static electromagnetic force on the coil was investigated with a series of currents applied to the coil. The opening and closing force were evaluated by applying the current in opposite directions and the effect on the opening and closing operations was also determined. It was assumed that the maximum coil current was 50 A. Fig. 6 shows the comparison of the flux density in the airgap produced solely by the magnets and including the flux density from the actuator coil carrying 50 A in both directions.

When the actuator current is in the anti-clockwise direction, the magnetic field in the inner steel cylinder was increased because the coil field was acting in the same direction as the magnet field. In this case the actuator coil was subjected to a downward force along the negative Z-axis providing the force to open the VI. The variation of the airgap flux density including the coil flux density displays the classical effect of armature reaction with the magnetic field increasing at the top because of the field produced by the actuator coil and reducing slightly at the bottom because part of the steel magnetic circuit has become saturated by the increased magnetic field produced by the actuator coil. The actuator coil receives a downward force of 882 N at the top position. The force produced for a 5 mm coil displacement varies from 882 N to 875 N. This confirms that the linear actuator provides a nearly constant force along its whole displacement.

When the actuator current is in the clockwise direction, the magnetic field in the airgap at the top of the path is reduced by the current in the actuator coil and is slightly increased at the bottom. A vertical force of 547 N moves the actuator coil upwards closing the vacuum circuit breaker. The closing force of 547 N is much lower than the opening force of 875 N for the same coil current and this will be analyzed next.

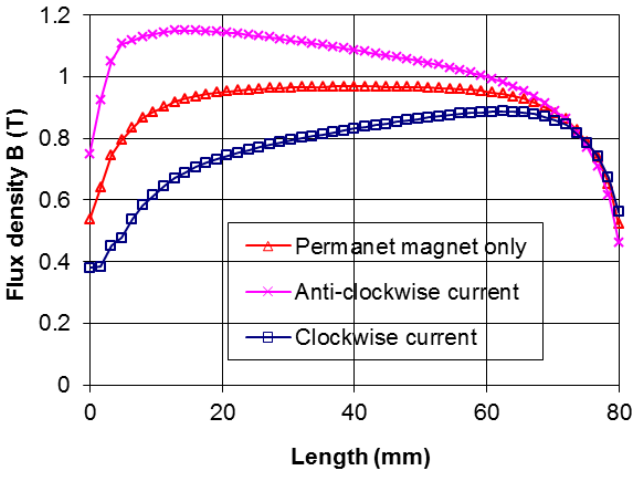

Fig. 6. Flux density distribution in the airgap with the actuator coil carrying 50 A in both directions (along the vertical path).

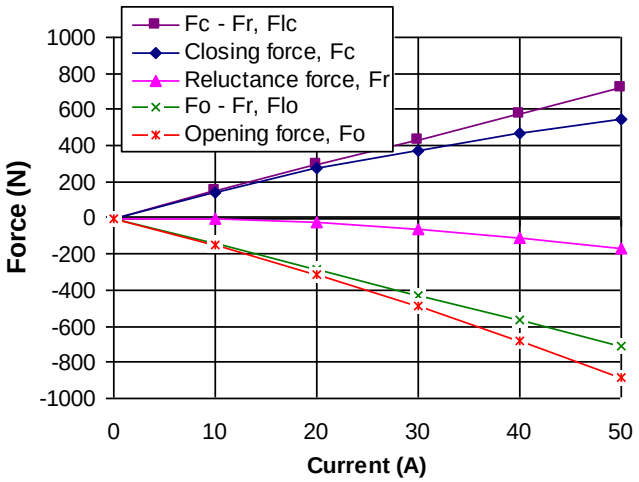

Fig. 7. Actuator force versus current characteristics.

The current in the actuator coil was varied from 10 A to 50 A, in steps of 10 A, for both the clockwise and anti-clockwise directions. The force variation on the actuator coil is illustrated in Fig. 7, showing that for the same current, the magnitude of the force to open the actuator, Fo, is consistently higher than that to close the actuator, Fc. The difference between the opening force and closing force is due to axial asymmetry in the magnetic structure of the actuator and results in a reluctance force component, Fr, which is also shown in Fig. 7. The reluctance force shown in Fig. 7 was confirmed and calculated by the FE model by setting the properties of the permanent magnet material to that of air. For the chosen coordinate definition, the reluctance force always acts along the negative Z-axis pushing the coil down towards the bottom steel plate. This is independent of the current direction but increases closely to the square of the coil current, as expected. The force to open the actuator is the Lorentz force on the coil plus the reluctance force and they are in the same direction whilst the force to close the actuator is in the opposite direction to the Lorentz force on the coil. This explains why the force to open the vacuum circuit breaker is always higher than the force to close it at the same current level. The magnitude of the Lorenz force on the coil when opening, Flo, and closing, Flc, are the same. The higher opening force for the same current is beneficial however for operating the VI because the opening velocity and time is more critical in most applications. The reclosing speed of the VI is normally of less concern.

C. Magnetic latch design

The actuator does not have an inherent stable position when the power supply to the actuator coil is removed. It is important that if the contacts are in the open or closed position, the actuator is safely secured in that position. Magnetic latches at both ends were employed therefore to hold the actuator in position, as shown in Fig. 8. The top magnetic latch was made from a steel plate, a magnet and a latch steel. The steel plate was fixed at the top of the outer steel wall, forming part of the low reluctance path for the top latch. The top latch magnet was placed beneath the steel plate. The latch steel was then placed between the top latch magnet and the main magnet. The latching force at the top (closed position) was provided by the top latch magnet, whilst the latching force at the bottom (open position) was provided by the main magnet.

The magnetic latches were added into the FE model to estimate the latching force because the latch magnetic circuit is complex and non-linear. It was found that the magnetic field in the airgap between the magnet and the latch steel is higher when the latch steel is at the top position. The latch steel therefore was designed to have a bigger area at the bottom than the top, as shown in Fig. 8 (right), to increase the latching force at the bottom position. The force on the latch steel was calculated using a Maxwell stress tensor over the surface surrounding it. The latching force from one latch at the top was 52 N. Two top latches were employed to keep the actuator mechanically balanced. They would provide a force of 104 N in total, which was more than enough to hold the interrupter in the closed position. Four sets of latches at the bottom position were used: two of these contained the top latch magnets. The latching force from those with the top latch magnets was 14 N, whilst for the latches without the top latch magnets it was 24 N; therefore, the total latching force in the open position would be 38 N.

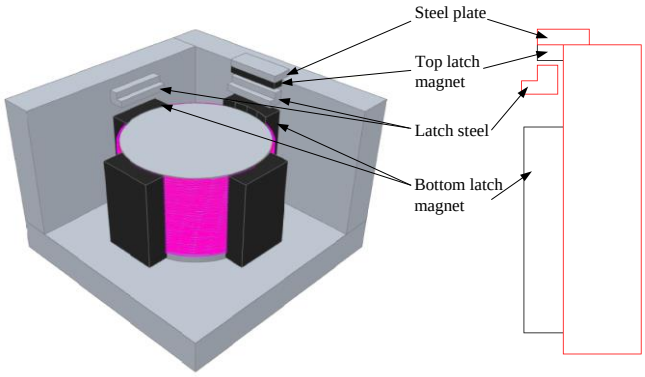

Fig. 8. Geometry of the actuator with magnetic latch (left) and cross-sectional view (right)

D. Design of final operational actuator

To design a high performance operating actuator for the VI, many factors need to be considered such as contact popping, bounce, rebound and welding [5]. The reasons for these problems and how to design the operating actuator to satisfy the requirements are discussed here.

In order to prevent contact popping when a current passes through the contacts, a minimum static contact holding force is usually required. The common way to provide this force is to place a spring along the driving shaft near the VI. The spring is pre-compressed (commonly called the wipe spring) in order to provide a considerable force immediately after the contacts are closed. During normal operation, the contacts would gradually wear and erode. The compression of the spring and holding force are then reduced, so the pre-compression of the spring helps minimize this reduction [5]. The required contact holding force for a DVS10CB VI is 2 kgf when the contacts carry 3.2 kA. The wipe spring with a stiffness of 2 N/mm

therefore is placed next to the movable contact. The spring is pre-compressed by 10 mm, so a force of 20 N is placed on the closed contacts. To provide the holding force reliably, the stroke of the actuator is designed to be 5 mm, which is 3 mm further than the stroke of the VI. An extra force of 6 N therefore exists on the contacts when the actuator is in the closed position.

Contact bounce on closing is undesirable because it can cause arcing when the contacts separate. A flexible supporting spring is placed next to the stationary contact of the vacuum circuit breaker to minimize contact bounce [5, 23]. The stiffness of the spring has to comply with the following equation [5]:

$$K < \frac{[(1+M_2/M_1)^2 - 1](1+M_2/M_1)F^2}{M_1 v_{10}^2} \quad (6)$$

where K is the spring stiffness, F is the resultant force on the vacuum circuit breaker in the closed position, v_{10} is the initial velocity of the moving contact before collision, M_1 and M_2 is the mass of the moving and stationary part, respectively.

A compression spring with a stiffness of 5 N/mm was placed therefore between the interrupter stationary contact and the supporting plate, forming a flexible support structure to absorb the kinetic energy and avoid contact bouncing.

Contact rebound on opening is a similar problem to contact bounce. If the rebound brings the contacts close to each other again, the dielectric recovery of the vacuum circuit breaker could be compromised. The movable contact therefore must be stopped and held at the end of the opening stroke. To ensure the movable contact does not rebound, the kinetic energy has to be absorbed at impact. Building some dissipative element into the mechanical stopper is feasible. In this prototype, contact opening rebound is overcome using the magnetic latches to provide an adequate holding force and a rubber pad as a damper.

Arcing caused by contact popping and bouncing will eventually melt the surfaces of the contacts, and this may form a weld when the contacts come together. Although the expected interrupting current level is much lower than its maximum value, contact welding is still unavoidable. It is necessary therefore to build a mechanism to break any contact weld when opening the vacuum circuit breaker. A snatch bracket is placed between the actuator and the wipe spring to fracture contact welding. During the process of closing the vacuum circuit breaker, the actuator travels further after the contacts are closed, to compress the wipe spring and provide the holding force to avoid popping. When the vacuum circuit breaker opens, the actuator has to travel back the same distance before the contacts separate. When the contacts start to separate, a significant amount of kinetic energy therefore has already accumulated in the moving part of the mechanism. This energy is used to fracture the welding by snatching the moving contact and pulling it away from the stationary contact.

The geometry of the 3-D structure of the operating actuator with vacuum circuit breaker, which consists of an actuator, magnetic latches, a snatch bracket, a driving shaft, a wipe spring and a supporting structure, is shown in Fig. 9.

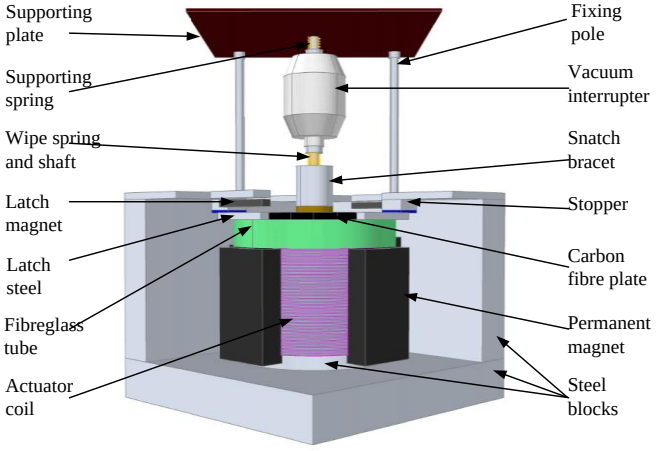

Fig. 9. 3-D structure of the operating actuator

IV. Experimental Setup and Verification

Following the detailed design, a prototype operating actuator was built. Fig. 10 (a) shows the prototype actuator coil with 79 turns wound on a fiberglass tube. Fig. 10 (b) shows the steel frame with the magnets assembled along each side. The assembled prototype actuator with the VI is shown in Fig. 10 (c).

An actuator control circuit was also designed to control the operation of the VI. Fig. 11 shows a schematic diagram of the actuator control circuit. The power supply for the actuator was provided using a set of pre-charged capacitors. The actuator coil was connected to the pre-charged capacitors through a single phase full-bridge DC-DC converter to control the coil voltage and current. MOSFETs (G1 to G4) were selected because they are suitable for low voltage and low current applications. The DC bus capacitor C1 was pre-charged to a voltage between 50 V and 150 V by a DC power supply to provide the energy to open and close the VI.

Fig. 12 shows a photo of the test rig of the actuator prototype, including a fast speed camera Photron Fastcam SA-X2, the capacitors, the moving coil actuator and its control circuit. The fast speed camera, which offers 1024 horizontal × 1024 vertical resolution and 12,500 frames per second, was used to accurately record the displacement of the actuator during operation. The voltage across the capacitors and the current through the actuator coil was also recorded by a high sampling rate oscilloscope.

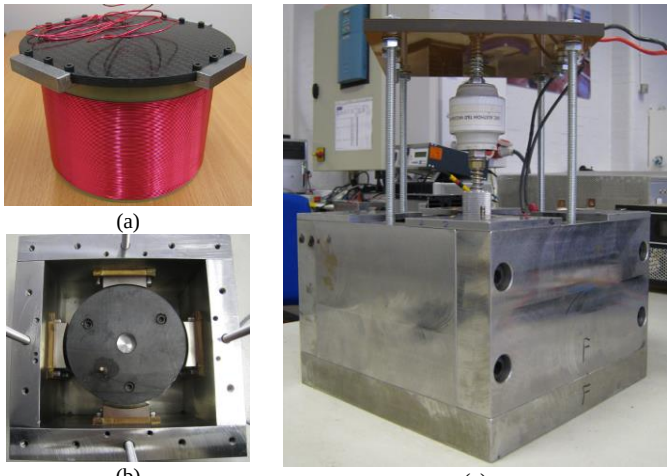

Fig. 10. Moving coil actuator prototype: (a) actuator coil on the fibreglass tube, (b) steel frame with permanent magnets, and (c) prototype actuator with vacuum circuit breaker.

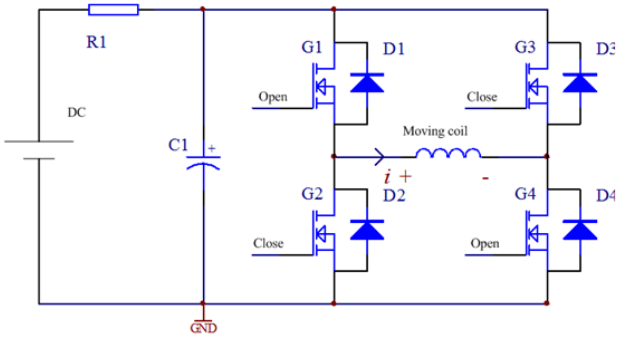

Fig. 11. Schematic diagram of the actuator control circuit.

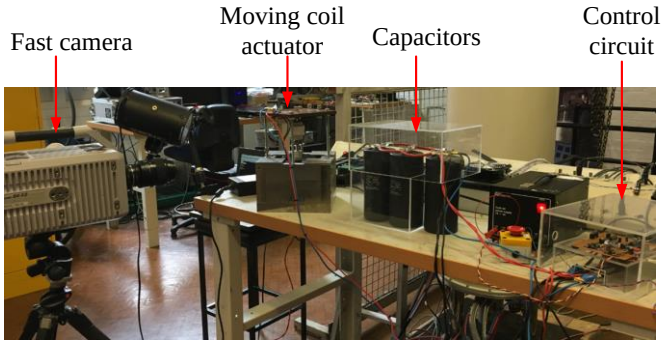

Fig. 12. Actuator prototype test setup.

A. *Actuator magnetic field and static force*

The magnetic field distribution in the actuator plays an important role in the behaviour of its operation. When the steel blocks and the permanent magnets were assembled, as shown in Fig. 10 (b), the magnetic flux density in the airgap between the central steel cylinder and the permanent magnets was measured using a Gauss meter. The magnetic flux density at the center of each magnet at the airgap varied from 0.95 T to 1.04 T. The maximum magnetic flux density at each side was slightly different due to airgap tolerance. The maximum magnetic flux density obtained from the FE model was 0.965 T. The experimental measurements were within ± 5% of the FE model, which shows good correlation. The experimental measurements also revealed that the magnetic flux density at the center of the permanent magnets was higher than at the magnet edges and also predicted by the FE model.

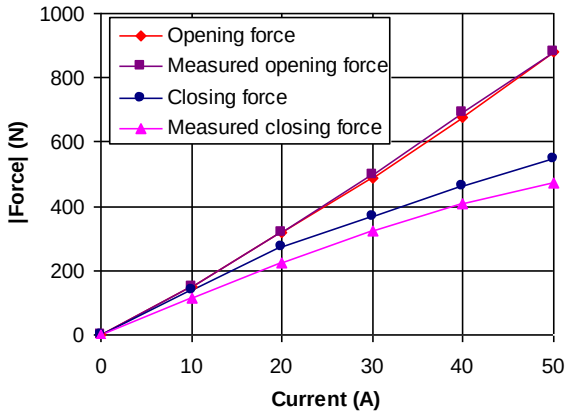

Fig. 13. Actuator opening and closing force versus current.

The actuator coil was placed in the airgap after the static magnetic field measurements. The static opening force and closing force were measured using an S-type load cell with the applied current level increasing from 10 A to 50 A. The measured opening and closing forces together with the predicted forces from the FE model are shown in Fig. 13. It is clear that the measured opening and closing forces again exhibit a good correlation with the FE model. The measured closing force is approximately 10% lower than the predicted force, which is within the measurement error bands associated with the mechanical implementation of the force sensing transducer (i.e. transducer mass and stiffness). The force measurement demonstrates that the opening force is higher than the closing force as a direct consequence of the asymmetry in the actuator reluctance. This additional reluctance force which was designed to increase the opening force is a desirable feature in terms of the objective of opening the VI as quickly as possible [4].

B. *Actuator opening operation*

Opening the VI is more critical than closing. If the VI could open faster when a fault occurs, less energy would be dissipated in the equipment in the fault network. The opening operation of the VI therefore was carefully evaluated.

During the opening operation, the actuator was activated using its control circuit and powered by the capacitors shown in Fig. 12. The current duration in the actuator coil for opening the vacuum circuit breaker was set at 10 ms at atmospheric pressure. The opening of the vacuum circuit breaker was tested with the capacitor voltage of 50 V. The test was repeated by increasing the capacitor voltage step by step up to 150 V. Fig. 14 shows the voltage across the capacitors, current through the actuator coil, linear displacement and velocity of the actuator coil for different capacitor pre-charge voltages. The displacement of the actuator coil was measured using the fast speed camera because the camera could capture the movement accurately without direct contact. Automatic video tracking software was used to determine the actuator displacement versus time characteristics and the velocity was estimated by numerical differentiation of the actuator displacement.

As shown in Fig. 14, the voltage across the capacitors is reducing during the 10 ms opening operation because energy is

converted to mechanical energy and also dissipated in the actuator coil. The current through the actuator coil initially increases steadily when the velocity of the actuator coil is relatively low. The current then becomes relatively stable when the velocity is high due to the back emf. The current increase again when the actuator coil achieves its maximum displacement.

The displacement of the actuator coil in Fig. 14 shows that the actual actuator stroke increased slightly to 5.5 mm because of compression of the rubber pad on the stopper. It takes around 9.5 ms, 6.3 ms, 5.5 ms, 4.7 ms and 4.2 ms, respectively, with capacitor voltages of 50 V, 80 V, 100V, 120 V and 150 V to fully open the VI. It is clear that a higher voltage on the capacitors produces a higher current in the actuator coil and opens the vacuum circuit breaker in a shorter period of time. The reduction of the opening time becomes less significant as the capacitor voltage increase.

The velocity of the actuator was derived from the displacement using a zero-lag running average algorithm and a smooth noise-robust numerical differentiator to reduce sudden variations. Actuator rebound is clearly observed in Fig. 14 as the velocity increases again after it reaches zero and is more significant with higher capacitor voltages. Further investigation is needed to determine if the contacts of the VI rebound as well.

The efficiency of this moving coil actuator prototype was calculated using equation 5. The maximum velocity was 1 m/s at 6 ms when the capacitor was charged to 50 V. The capacitor voltage itself reduced from 50 V to 45 V. The efficiency was approximately 9% when the capacitor was charged to 50 V increasing to 12% when the capacitor was charged to 150 V. One possible reason for the low efficiency was that the resistance of the actuator coil was high due to the use of small diameter copper wire to maintain a small airgap. The efficiency is relatively low, but the operation of opening and reclosing the actuator three times could be achieved by the energy stored in the capacitors.

The actuator and VI was originally proposed to be directly integrated into the vacuum of a cryostat system used for a superconducting fault current limiter [4]. The actuator was therefore tested in the vacuum chamber with a pressure of 1.4×10^{-3} mbar. The comparison of opening the VI at atmospheric pressure and in the vacuum is illustrated in Fig. 15. Fig. 15 presents the voltage across the capacitors, current through the actuator coil and linear displacement of the actuator coil when the vacuum circuit breaker opens. It was not possible to use the camera in the vacuum chamber due to the limited space. In this test the displacement of the actuator coil was measured using a DFg5 unguided miniature linear variable differential transformer (LVDT). The response time constant of the DFg5 LVDT was about 3 ms, so the displacement is time-shifted by 3 ms in Fig. 15.

The opening operation at atmospheric pressure and in the vacuum can be separated into the following periods:

0-t1: The current through the actuator coil is similar in both pressure conditions because the velocity of the moving coil is relatively slow.

t1-t2: The actuator coil starts to accelerate faster in the vacuum than at atmospheric pressure because of the reduced air resistance. The displacement of the actuator coil in the vacuum is therefore higher. In the vacuum, a higher velocity induces a higher back electromotive force and hence a lower current in the actuator coil.

t2-t3: In the vacuum, the contacts start to separate when the displacement is 3 mm. The coil current in the vacuum reduces quicker compared to atmospheric pressure due to the higher velocity and hence higher back emf.

t3-t4: At atmospheric pressure, the contacts start to separate. To provide the force to open the VI, the velocity of the moving coil decreases and the coil current increases steadily. The coil current increases faster when the actuator is in the vacuum than at atmospheric pressure because the back emf decreases quicker. The contacts are fully opened in the vacuum when a 5 mm displacement has been achieved and the current increases to its maximum level. The opening time in the vacuum is approximately 5 ms.

t4-t5: At atmospheric pressure, the contacts are fully open when the current increases to its maximum level. The opening time at atmospheric pressure is approximately 5.5 ms.

t5-: The current drops to a steady state level before the supply is removed. At atmospheric pressure, the current in the actuator coil lasts for 10 ms. In the vacuum, the current duration increases to 15 ms to keep it in the open position for a longer period of time and reduce any possibility of rebound due to the reduced air resistance.

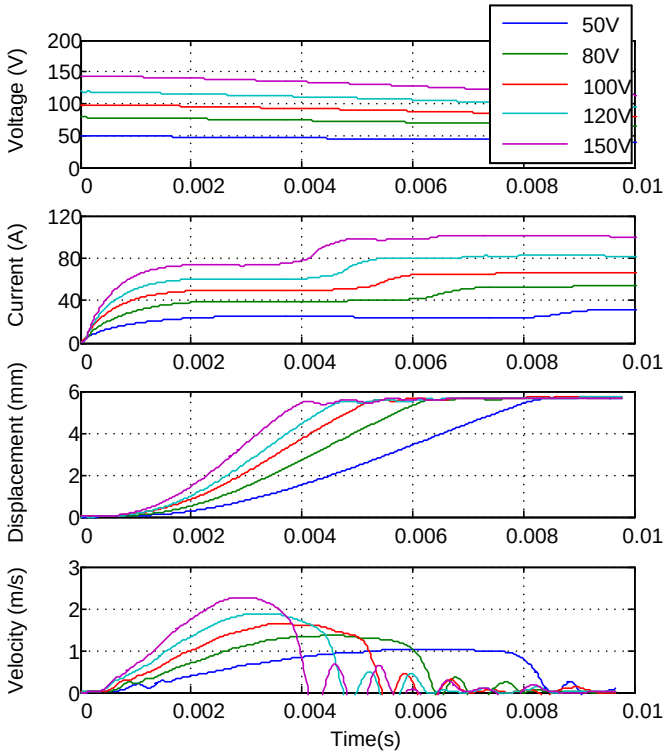

Fig. 14. Actuator opening operation with different capacitor voltages.

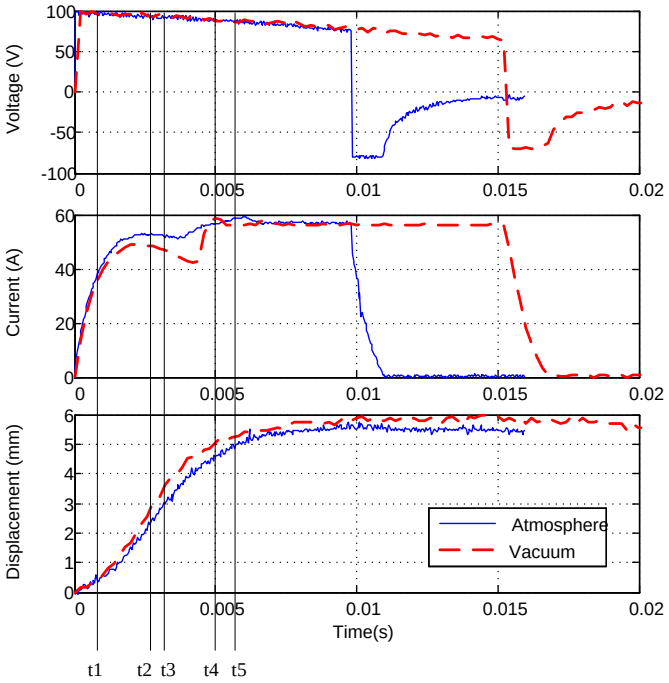

Fig. 15. Opening operation of the vacuum circuit breaker at atmospheric pressure and in the vacuum.

It is clear from the displacement curve that opening in the vacuum is faster than at atmospheric pressure. This is an additional benefit to integrating the actuator with the vacuum circuit breaker into the vacuum system.

C. Performance improvement

The performance of the prototype moving coil actuator can be improved in terms of operating speed and efficiency. A variety of aspects are considered for optimizing its performance:

- Minimizing the moving mass can improve both the operating speed and efficiency.
- Increasing the input energy by increasing the initial capacitor voltage or capacitance can result in an increase in the operating speed. As demonstrated in the experimental test, the operating speed was increased as the capacitor pre-charge voltage increases.
- Increasing the number of coil turns results in an increase in efficiency. The increased inductance however will increase the time constant of the actuator coil and hence reduce the operating speed. The inductance of the coil can be reduced by breaking the coil into several parallel connected coils instead of one series connected coil.
- Reducing the resistance of the actuator coil to cut the electrical energy consumption can increase the efficiency of the actuator. This can be achieved by increasing the cross-sectional area of the actuator coil. Square copper wire could be considered due to the limited axial length of the airgap. The reduction of resistance however will increase the time constant of the actuator coil and hence reduce the operating speed.

The optimization procedure would involve evaluation of both the operating speed and efficiency, and would also depend on each application, with a focus on which parameter is more important.

V. Conclusions

A high-speed moving coil actuator was simulated using an FE model and a prototype high performance operating actuator was built and experimentally tested. The measured opening and closing forces show good correlation with the FE model. The prototype actuator demonstrated successful and repeated opening operating of the vacuum circuit breaker with magnetic latches holding the actuator in the open position. The actuator opened a VI within 5 ms in a vacuum chamber and 5.5 ms at atmospheric pressure with a capacitor voltage of 100 V. We built this actuator and it demonstrated that the moving coil actuator can provide fast operation of the VI and latching functions in the open and closed positions without consuming electric energy. Further recommendations to enhance the performance of the moving coil actuator in respect of the operating speed and efficiency were summarized. This high-speed moving coil actuator shows significant potential and would be attractive for medium voltage network applications.

VI. References

[1] P. Picot, “Vacuum Switching,” Schneider Electric, Cahier technique no.198, 2000.

[2] S. Lim, H. Ahn, and C. Park, “Study on fault current limiting characteristics of a SFCL using magnetic coupling of two coils with mechanical switch driven by electromagnetic repulsion force,” *IEEE Trans. Appl. Supercond.*, vol. 24, no. 3, Jun. 2013, Art. ID 5600704.

[3] S. Husband, A. C. Smith, R. Shuttleworth, X. Pei, “Current limiter,” Patent number: EP 2621043 A2, Jul, 31, 2013.

[4] X. Pei and A. C. Smith, "Experimental tests of a resistive SFCL integrated with a vacuum circuit breaker," *IEEE Trans. Appl. Supercond.*, vol. 26, April, 2016.

[5] A. Greenwood, *Vacuum switchgear*, Stevenage: Institution of Electrical Engineers, 1994.

[6] K. Y. Ahn, and S. H. Kim, ‘Modeling and analysis of a high-speed circuit breaker mechanism with a spring-actuated cam,’ in *Proc. Inst. Mech. Eng. C J. Mech. Eng. Sci.*, vol. 215, pp. 663-672, Jun. 2001.

[7] W. Wen, Y. Huang, M. Al-Dweilat, and Z. Zhang, “Research on operating mechanism for ultra-fast 40.5-kV vacuum switches,” *IEEE Trans. Power Del.*, vol. 30, pp. 2553-2560, Nov. 2015.

[8] B. Lequesne, “Fast-acting long-stroke bistable solenoids with moving permanent magnets”, *IEEE Trans. Ind. Appl.*, vol. 26, pp. 401-407, May. 1990.

[9] B. Lequesne, “Fast-acting long-stroke solenoids with two springs”, *IEEE Trans. Ind. Appl.*, vol. 26, pp.848-856, Sep. 1990.

[10] B. I. Jung and H. S. Choi, “Combined effect of the SFCL and solenoid coils,” *IEEE Trans. Appl. Supercond.*, vol. 24, Jun. 2014, Art. ID. 5600404.

[11] H. Jiang, R. Shuttleworth, B. A. T. Al Zahawi, A. Power, “Variable speed latching magnetic actuator for a vacuum switch,” in *8th Int. Conf. Electrical Machines and Drives*, Cambridge, UK, Sep. 1997.

[12] E. Dullni, “A vacuum circuit-breaker with permanent magnetic actuator for frequent operations,” in *18th Int. Symp. Discharges Elect. Insul. in Vacuum*, Eindhoven, Netherlands, August 1998, pp. 688-691.

[13] S. Fang, H. Lin, and S. L. Ho, “Transient co-simulation of low voltage circuit breaker with permanent magnet actuator,” *IEEE Trans. Magn.*, vol. 45, pp.1242-1245, Mar. 2009.

[14] S. Fang, Q. Liu, H. Lin, and S. L. Ho, “A Novel Flux-Weakening Control Strategy for Permanent-Magnet Actuator of Vacuum Circuit Breaker,” *IEEE Trans. Ind. Electron.*, vol. 63, pp. 2275-2283, Mar. 2016.

[15] T. Takeuchi, K. Koyama, and M. Tsukima, “Electromagnetic analysis coupled with motion for high-speed circuit breakers of eddy current

repulsion using the tableau approach," *Electrical Engineering in Japan*, vol. 152, pp. 8-16, 2005.
[16] M. Tsukima, T. Takeuchi, K.Koyama, and H. Yoshiyasu, "Development of a high-speed electromagnetic repulsion mechanism for high voltage vacuum circuit breakers," *Electrical Engineering in Japan*, vol. 163, pp. 34–40, 2008.
[17] A. Bissal, J. Magnusson, G. Engdahl, "Comparison of two ultra-fast actuator concepts," *IEEE Trans. Magnetics*, vol. 48, pp. 3315-3318, Nov. 2012.
[18] A. Bissal, J. Magnusson, G. Engdahl, "Electric to mechanical energy conversion of linear ultrafast electromechanical actuators based on stroke requirements," *IEEE Trans. Ind. Appl*, vol. 51, pp. 3059-3067, Jul. 2015.
[19] D. S. Vilchis-Rodriguez, R. Shuttleworth, and M. Barnes, "Finite element analysis and efficiency improvement of the Thomson coil actuator," presented at 8th IET international conference on Power Electronics, Machines and Drives, Glasgow, UK, Apr. 2016.
[20] J. Borwick, *Loudspeaker and headphone handbook*, London: Butterworths, 1988.
[21] J. R. Brauer, *Magnetic actuators and sensors*, (2nd ed.), Hoboken, New Jersey: Wiley-IEEE Press, 2013.
[22] D. S. Vilchis-Rodriguez, R. Shuttleworth, and M. Barnes, "Finite element assessment of moving coil actuator for HVDC breaker applications" presented at The 42nd Annual Conference of the IEEE Industrial Electronics Society (IECON2016), Florence, October 24-27, 2016.
[23] P. Barkan, "A study of the contact bounce phenomenon," *IEEE Trans. Power App. Syst*., vol. PAS-86, pp. 231-240, 1967.

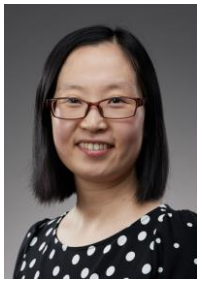

X. Pei received the B.Eng. and M.Eng. degrees from Beijing Jiaotong University, Beijing, China in 2006 and 2008, respectively. She received the Ph.D. degree from the University of Manchester, Manchester, U.K. in 2012. She became a Research Associate at the University of Manchester. In 2017, she joined the University of Bath as a Lecturer. She has extensive research experience in designing and building of superconducting fault current limiters and fast operating circuit breakers. Her research interests include electrical power applications of superconductivity and renewable energy integrations.

A. C. Smith (M'89–SM'02) received the B.Sc. (Eng) and Ph.D. degrees from Aberdeen University, Aberdeen, U.K., in 1977 and 1980, respectively.
He has held academic appointments at Imperial College, London, U.K.(1983–1990), and Cambridge University, Cambridge, U.K. (1990–1997). In 1997, he joined Invensys Brook Crompton, Huddersfield, U.K., as Head of Research responsible for motor technology. In 2000, he joined the University of Manchester Institute of Science and Technology, Manchester, U.K., as a Senior Lecturer, as a Reader in Electrical Machines in 2003, and as a Professor of Electrical Machines in 2007. In 2004, he was appointed the Director of the Roll-Royce University Technology Centre on Power Conversion at the University of Manchester. His research interests include design and modelling of motors, generators, and drives.
He is a Fellow of the Institute of Engineering and Technology (formerly IEE), U.K., and is currently the Editor of the IET Journal Electrical Systems in Transportation

R. Shuttleworth (M'07) was born in the UK and completed his BSc and PhD degrees in Electrical and Electronic Engineering at The University of Manchester. He worked for a year at GEC Traction before joining the University as a lecturer in the Power System's Research group and later the Power Conversion Research group. He has around 100 papers and patents and was Director for the Power Electronics, Machines and Drives MSc course at Manchester University until 2016.
His main research activities are in the areas of Power Electronics, Energy Control and Conversion, HVDC, circuit breaking, and Energy Harvesting.

D. S. Vilchis-Rodriguez (M'10) received the Ph.D. degree in electrical engineering from the University of Glasgow, Glasgow, U.K., in 2010. He was a computer programmer and power quality consultant in Mexico for the period 1993-2004. He is currently a Research Associate with the Power & Energy Division, University of Manchester, Manchester, U.K. His current research interests include electrical machines modelling, condition monitoring, power systems dynamics simulation and high voltage dc protection.

M. Barnes (M'96–SM'07) received the B.Eng. and Ph.D. degrees in power electronics and drives from the University of Warwick, Coventry, U.K., in 1993 and 1998, respectively. In 1997, he was a Lecturer with the University of Manchester Institute of Science and Technology, Manchester, U.K. (UMIST merged with The University of Manchester). He is currently Professor of Power Electronics Systems at The University of Manchester. His research interests cover the field of power-electronics-enabled power systems.